The Plant Cell, Vol. 19: 4007–4021, December 2007, www.plantcell.org © 2007 American Society of Plant Biologists

The *Arabidopsis MUM2* Gene Encodes a β-Galactosidase Required for the Production of Seed Coat Mucilage with Correct Hydration Properties [W]

Gillian H. Dean,[a] Huanquan Zheng,[a,1] Jagdish Tewari,[b,2] Jun Huang,[a] Diana S. Young,[a] Yeen Ting Hwang,[a] Tamara L. Western,[a,1] Nicholas C. Carpita,[c] Maureen C. McCann,[b] Shawn D. Mansfield,[d] and George W. Haughn[a,3]

[a] Department of Botany, University of British Columbia, Vancouver, Canada V6T 1Z4
[b] Department of Biological Sciences, Purdue University, West Lafayette, Indiana 47907
[c] Department of Botany and Plant Pathology, Purdue University, West Lafayette, Indiana 47907
[d] Department of Wood Science, University of British Columbia, Vancouver, Canada V6T 1Z4

Seed coat development in *Arabidopsis thaliana* involves a complex pathway where cells of the outer integument differentiate into a highly specialized cell type after fertilization. One aspect of this developmental process involves the secretion of a large amount of pectinaceous mucilage into the apoplast. When the mature seed coat is exposed to water, this mucilage expands to break the primary cell wall and encapsulate the seed. The *mucilage-modified2* (*mum2*) mutant is characterized by a failure to extrude mucilage on hydration, although mucilage is produced as normal during development. The defect in *mum2* appears to reside in the mucilage itself, as mucilage fails to expand even when the barrier of the primary cell wall is removed. We have cloned the *MUM2* gene and expressed recombinant MUM2 protein, which has β-galactosidase activity. Biochemical analysis of the *mum2* mucilage reveals alterations in pectins that are consistent with a defect in β-galactosidase activity, and we have demonstrated that MUM2 is localized to the cell wall. We propose that MUM2 is involved in modifying mucilage to allow it to expand upon hydration, establishing a link between the galactosyl side-chain structure of pectin and its physical properties.

INTRODUCTION

The secretion of large amounts of mucilage in a specialized cell type makes the seed coat an excellent model system for studying aspects of polysaccharide biosynthesis, secretion, and modification. The development of the *Arabidopsis thaliana* seed coat has been studied in detail (Beeckman et al., 2000; Western et al., 2000; Windsor et al., 2000). After fertilization, the cells of the outer ovule integument secrete a large amount of pectinaceous mucilage into the apoplast. This secretion is targeted to the junction of the radial and outer tangential cell walls, resulting in a mucilage-filled apoplastic domain surrounding a volcano-shaped cytoplasm. After mucilage secretion, the secondary cell wall is deposited and eventually fills the entire space occupied by the cytoplasmic column. Therefore, mature seed coat cells of *Arabidopsis* consist of a volcano-shaped secondary cell wall known as the columella surrounded by a donut-shaped ring of mucilage.

When mature seeds are hydrated, the outer radial wall breaks and the mucilage is extruded to form a capsule around the seed. Although it has been proposed that seed mucilage may be important for germination under conditions of water stress in *Arabidopsis* (Penfield et al., 2001), mucilage production and seed coat differentiation are dispensable under laboratory conditions. This feature, as well as the availability of a simple screen that uses Ruthenium Red to stain acidic pectins (Hanke and Northcote, 1975) found in extruded mucilage, allows for relatively straightforward identification of mutants with defects in mucilage biogenesis (Western et al., 2001).

Arabidopsis mucilage is composed primarily of pectin (Western et al., 2000, 2004; Penfield et al., 2001; Usadel et al., 2004; Macquet et al., 2007a, 2007b). Pectins are a group of complex and structurally diverse polysaccharides, with two key pectins being homogalacturonan (HG) and rhamnogalacturonan I (RG-I; O'Neill and York, 2003). HG is structurally related to xylogalacturonan and rhamnogalacturonan II (RG-II); all have a backbone of (1→4)-α-D-galacturonic acid residues, with HG being unbranched, xylogalacturonan being substituted with xylose residues, and RG-II having complex but structurally defined, nonvariable side chains. By contrast, RG-I has a backbone consisting of alternating (1→4)-α-D-galacturonic acid and (1→2)-α-L-rhamnose with variable side chains containing arabinose, fucose, galactose, and glucuronic acid.

Pectin has been ascribed important roles in ion transport, molecular sieving, and cell adhesion because of its physical properties (Knox, 2002) and is also a potential source of

[1] Current address: Department of Biology, McGill University, Montreal, Canada H3A 1B1.
[2] Current address: Department of Fiber Science and Apparel Design, Cornell University, Ithaca, NY 14853.
[3] Address correspondence to haughn@interchange.ubc.ca.
The author responsible for distribution of materials integral to the findings presented in this article in accordance with the policy described in the Instructions for Authors (www.plantcell.org) is: George W. Haughn (haughn@interchange.ubc.ca).
[W] Online version contains Web-only data.
www.plantcell.org/cgi/doi/10.1105/tpc.107.050609

oligosaccharides that can act as signaling molecules (Ridley et al., 2001). The structure of pectin determines these properties, and pectin structure is often modified in particular cell types (Knox, 2002) as well as during growth and developmental processes such as fruit ripening (Rose et al., 2003).

Arabidopsis seed mucilage is composed largely of relatively unbranched RG-I (Western et al., 2000, 2004; Penfield et al., 2001; Usadel et al., 2004; Macquet et al., 2007a, 2007b). Immunocytochemical studies also indicate that HG is present in mucilage (Willats et al., 2001a; Western et al., 2004; Macquet et al., 2007a, 2007b), and there is evidence that 4-linked glycans form a constituent of mucilage (Windsor et al., 2000; Willats et al., 2001a; Macquet et al., 2007a, 2007b; G.H. Dean and G.W. Haughn, unpublished data). Smaller amounts of sugar linkages associated with arabinoxylans and type II arabinogalactans are also detected (Penfield et al., 2001).

A number of mutants have been identified in which development of the seed coat is perturbed (Haughn and Chaudhury, 2005; Western, 2006). One subset of these mutants (*mucilage-modified1* [*mum1*], *mum2*, and *patchy*) appear to undergo normal epidermal cell differentiation and mucilage secretion, but mature seeds do not release mucilage on hydration (Western et al., 2001; T.L. Western, T.M. Popma, and G.W. Haughn, unpublished data). This defect in mucilage extrusion may reflect changes in the primary cell wall that prevent it from breaking or alterations in the ability of mucilage to hydrate and expand on contact with water.

Here, we present a phenotypic analysis of the cytological and biochemical defects in the *mum2* mutant. We show by positional cloning that the *MUM2* gene encodes the Family 35 β-galactosidase At BGAL6, which is localized in the apoplast and results in modified pectin side chains to enable increased hydration properties of mucilage.

RESULTS

mum2 Develops Normally but Does Not Release Mucilage on Hydration

When mature wild-type *Arabidopsis* seeds are exposed to water, mucilage is extruded from the epidermal cells to encapsulate the seed (Figure 1A). Screening a mutagenized population of M3 lines using Ruthenium Red as a stain identified a large number of mutants with altered seed coat mucilage (Western et al., 2001). Complementation tests identified nine mutant alleles of *MUM2* from four independent mutagenized populations. As all of the alleles have a similar phenotype, only the *mum2-1* allele will be described in detail.

The *mum2* mutant is characterized by a complete absence of extruded mucilage in hydrated seeds when examined by Ruthenium Red staining (cf. Figures 1A with 1B; Western et al., 2001). Scanning electron microscopy of mature, dry seeds revealed that *mum2* and the wild type are indistinguishable, indicating that the failure of *mum2* mucilage to be released on hydration is not associated with an obvious morphological defect (Figures 1C and 1D).

Developing seeds from *mum2* and wild-type plants were sectioned, stained with Toluidine Blue, and examined by light microscopy (Figures 1E to 1N). Between 4 and 13 d post-anthesis (DPA), *mum2* seeds were indistinguishable from the wild type, with mucilage deposition into the apoplast and columella formation appearing to proceed as normal (cf. Figures 1E to 1H with 1J to 1M; for a detailed description of seed coat epidermal differentiation, see Western et al., 2000). However, unlike the wild type, when 16-DPA *mum2* seeds are hydrated during the fixation process, the primary cell wall fails to break and no mucilage is extruded (cf. Figures 1I to 1N). Note that slight variations in staining intensity between different sections is within the bounds of normal Toluidine Blue staining and does not reflect differences in morphology or structure of cell components such as mucilage.

In mutants such as *mum4*/*rhm2* where less mucilage is produced (Usadel et al., 2004; Western et al., 2004) the morphology of epidermal cells tends to be altered. In the case of *mum2*, the normal appearance of the epidermal cells indicates that the lack of mucilage release is not due to a decrease in mucilage amount but is more likely due to a lack of mucilage release on hydration.

mum2 Seeds Can Release Mucilage on Hydration with Na_2CO_3

The release of mucilage during seed hydration is thought to involve the expansion of hydrophilic mucilage in the apoplast as it absorbs water, resulting in the breakage of the radial primary cell wall (Western et al., 2000). We investigated a number of chemical reagents and extractants for their ability to release mucilage from mature *mum2* seeds.

The chelating agents EDTA, EGTA, and CDTA (0.05 M concentration), which extract Ca^{2+}-cross-linked pectins, were able to extract a small amount of mucilage from *mum2* (Figure 1Q; see Supplemental Figure 1 online), whereas 0.5 M ammonium oxalate did not (see Supplemental Figure 1 online). Weak alkali, such as Na_2CO_3, has been reported to extract pectins by cleavage of cross-linking ester linkages (Selvendran and Ryden, 1990; Fry, 2000; McCartney and Knox, 2002). Treatment of *mum2* seeds with 1 M Na_2CO_3 caused the primary cell wall to break and mucilage to be extruded (cf. Figures 1R and 1B). Although it is apparent that the primary cell wall has broken (columellae can be visualized as dark staining points on the seed surface), *mum2* mucilage does not expand as much and does not stain as darkly with Ruthenium Red as wild-type mucilage (cf. Figures 1P and 1R).

Strong alkali, such as KOH, extracts cross-linking glycans from cellulosic microfibrils (Fry, 2000). However, *mum2* mucilage was not released by treatment with 2 M KOH or 0.5, 1, or 2 M NaOH (data not shown). Although strong alkali is expected to de-esterify pectins in the same way as Na_2CO_3, it also swells of cellulose microfibrils by disruption of hydrogen bonds that may entrap the mucilage. Finally, 5.5 M guanidine thiocyanate, an aqueous chaotrophic agent that solubilizes mannans and glucomannans (Fry, 2000), did not release *mum2* mucilage (data not shown).

mum2 Mucilage Cannot Expand Even When Exposed Directly to Water

The failure of *mum2* mutants to release mucilage on hydration with water may be caused by an alteration in the mucilage that

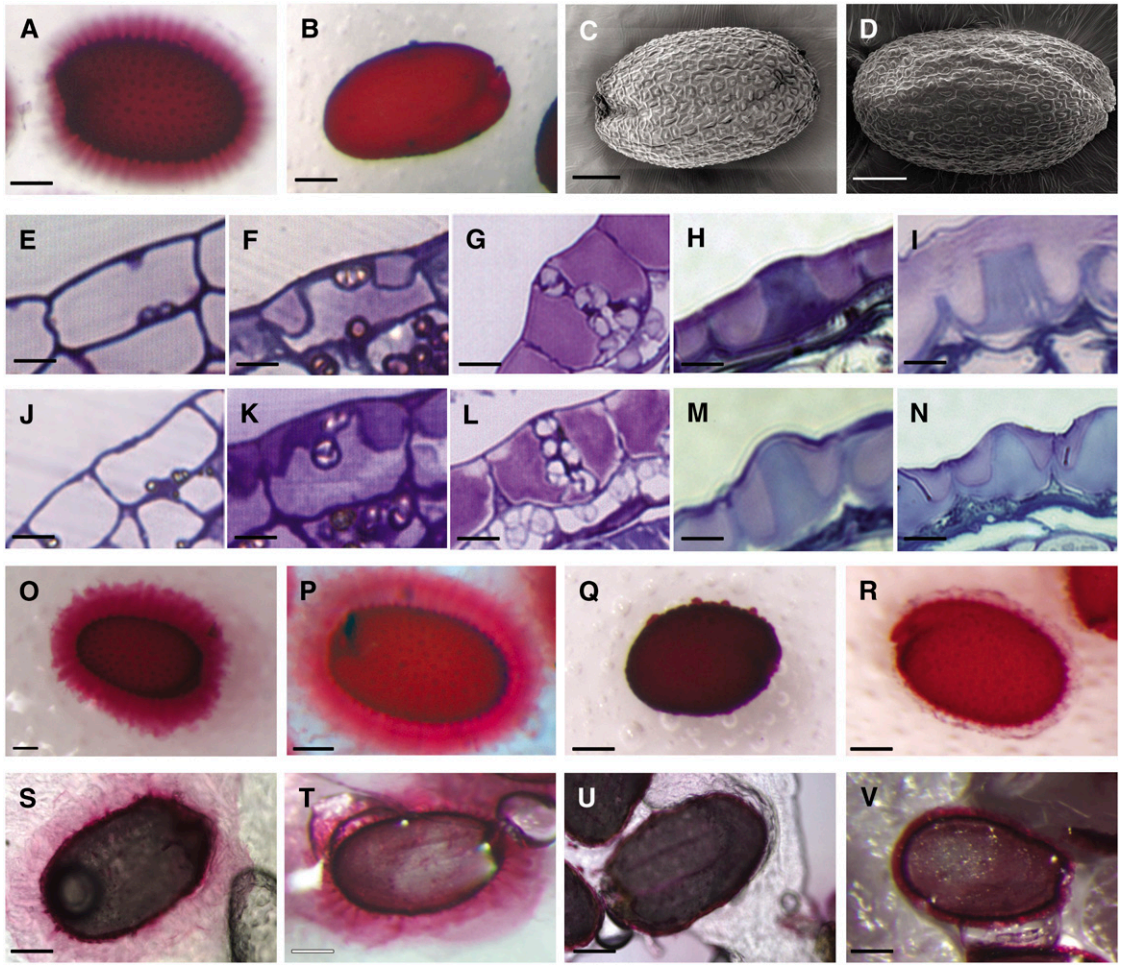

Figure 1. Cytological Analysis of the *mum2* Mutant.

(A) Mature wild-type seed stained with Ruthenium Red. A layer of stained mucilage is visible around the seed, and the columellae are clearly visible in the center of each cell, indicating that the outer tangential cell wall has ruptured.
(B) Mature *mum2* seed stained in Ruthenium Red. No extruded mucilage is visible, and the outer tangential cell walls have not ruptured.
(C) Scanning electron microscopy of mature wild-type seed. Hexagonal epidermal cells with thickened radial walls and a central columella are visible.
(D) Scanning electron microscopy of mature *mum2* seed. The mutant seeds are indistinguishable from the wild type.
(E) Wild-type seed coat epidermal cell at 4 DPA. Amyloplasts are visible; much of the cell volume is occupied by the vacuole.
(F) Wild-type seed coat epidermal cell at 7 DPA. Mucilage secretion into the apoplast has begun, and the cytoplasmic column is visible.
(G) Wild-type seed coat epidermal cell at 10 DPA. Mucilage secretion is complete, and columella formation has begun.
(H) Wild-type seed coat epidermal cell at 13 DPA. Columella formation is complete.
(I) Wild-type seed coat epidermal cell at 16 DPA. The epidermal cells of the seed coat have ruptured during the fixation process, and mucilage has been released. The columella and the radial cell walls are visible.
(J) to **(N)** The development of the *mum2* seed coat epidermal cells at 4 **(J)**, 7 **(K)**, 10 **(L)**, and 13 DPA **(M)** is indistinguishable from the wild type. However, at 16 DPA **(N)**, the *mum2* seed coat does not rupture and the mucilage remains within the primary cell wall (cf. **[I]** with **[N]**).
(O) and **(P)** Mature wild-type seed treated with EDTA **(O)** or Na_2CO_3 **(P)** and stained with Ruthenium Red. Mucilage has been released, and seeds have a similar appearance to those stained directly with Ruthenium Red (cf. with **[A]**).
(Q) Mature *mum2* seed treated with EDTA and stained with Ruthenium Red. Small amounts of mucilage are released from some cells.
(R) Mature *mum2* seed treated with Na_2CO_3 and stained with Ruthenium Red. A thin layer of poorly stained mucilage has been released. The columellae are visible, indicating that the outer tangential cell wall has ruptured (cf. **[R]** with **[B]**).
(S) and **(T)** Sections (20 μm) of mature, unfixed, paraffin-embedded wild-type seed hydrated with Ruthenium Red **(S)** or Na_2CO_3 and then Ruthenium Red **(T)**. The mucilage is extruded from the seed coat similar to intact seeds.
(U) Section (20 μm) of mature, unfixed, paraffin-embedded *mum2* seed hydrated with Ruthenium Red. The mucilage does not expand, despite being in direct contact with the aqueous dye solution.
(V) Section (20 μm) of mature, unfixed, paraffin-embedded *mum2* seed hydrated with Na_2CO_3 and then Ruthenium Red. The outer tangential cell wall has ruptured, and a thin layer of mucilage has been released, similar to intact seeds treated with Na_2CO_3.
Bars = 100 μm in **(A)** to **(D)** and **(O)** to **(V)** and 10 μm in **(E)** to **(N)**.

affects its ability to hydrate and/or changes in the seed epidermal primary cell wall that prevent it from breaking. To determine whether the *mum2* mucilage itself can hydrate, unfixed mature seeds of both wild-type and *mum2* mutants were embedded in paraffin wax and 20-μm sections prepared. Since seed coat epidermal cells are typically larger than 20 μm, few epidermal cells are intact in such sections, thereby eliminating the need for the mucilage to break the seed coat to expand. The sections were mounted on microscope slides and hydrated in the presence of Ruthenium Red. Wild-type sections prepared in this way showed hydration and expansion of the mucilage as in intact seeds (Figure 1S). By contrast, the *mum2* mucilage did not expand despite being in direct contact with the water with no apparent barrier to hydration (Figure 1U). We also hydrated wild-type and *mum2* sections with 1 M Na_2CO_3 prior to Ruthenium Red staining. In the wild type, expansion of mucilage occurs as in sections hydrated with Ruthenium Red directly (Figure 1T). In *mum2*, only a small amount of mucilage expansion was observed (Figure 1V), consistent with the hypothesis that the hydration of *mum2* mucilage itself is impaired. Although this experiment does not rule out the possibility that alterations in the primary cell wall also prevent breaking during hydration, these data indicate that the *mum2* mucilage itself is altered in its ability to hydrate and expand.

Cloning of the *MUM2* Gene

We identified the *MUM2* gene using positional cloning. The *MUM2* gene was localized on chromosome V between markers on BACs MBK5 and MHJ24. Of the 48 loci in this region, several were identified as putative carbohydrate active enzymes and selected as *MUM2* candidates. SALK insertion lines were obtained for these loci, and plants homozygous for an insertion in exon 3 of At5g63800 (SALK_011436) showed a *mum2* phenotype. The T-DNA insertion in this SALK line segregates with the *mum2* phenotype, and crosses to SALK_011436 failed to complement *mum2* (data not shown), indicating that At5g63800 is *MUM2* and SALK_011436 is homozygous for a T-DNA insertional allele (*mum2-10*).

The gene model for At5g63800 given at The Arabidopsis Information Resource (TAIR; www.arabidopsis.org) indicated that the gene consists of 16 exons and 15 introns. The first intron is especially large, at 1879 bp. Sequencing of At5g63800 genomic DNA from the fast neutron-generated *mum2-5* allele revealed a large deletion that eliminates most of intron 1 as well as all of exon 2. The coding sequence of At5g63800 comprises 2157 bases (GenBank accession number NM_125775). PCR amplification and sequencing of At5g63800 cDNA from wild-type 7-DPA siliques confirmed this coding sequence as well as the presence of 5′ and 3′ untranslated regions of at least 200 bases each. Sequencing of the At5g63800 cDNA from *mum2-1* and *mum2-2* revealed G-to-A transitions at 1537 and 713 bp, respectively. These mutations alter the amino acid sequence from Gly to Arg in *mum2-1* (residue 513) and from Gly to Glu in *mum2-2* (residue 238).

RT-PCR analysis on At5g63800 cDNA from these alleles reveals that transcript is present in *mum2-1*, *mum2-2*, and *mum2-5*. No transcript is present in the SALK allele *mum2-10* under our PCR conditions (Figure 2A). The base change in *mum2-1* is on an intron/exon boundary and also leads to inefficient splicing of the At5g6800 transcript as indicated by the presence of a larger PCR product containing the unspliced intron (Figure 2A, arrow).

To confirm that *MUM2* is encoded by At5g63800, molecular complementation of *mum2* was performed. A genomic DNA fragment spanning from 2 kb upstream of the At5g63800 ATG to 1 kb downstream of the At5g63800 stop codon was amplified by PCR, cloned into pCAMBIA1200 to create plasmid pMUM2g, and used to transform *mum2* plants. Empty pCAMBIA1200 was transformed into *mum2* plants as a control. From 30 independent lines transformed with pMUM2g, 26 showed complete rescue of the *mum2* phenotype (Figure 2B). None of 18 independent transformants carrying empty pCAMBIA1200 rescued the *mum2* phenotype (Figure 2C).

MUM2 Encodes a Putative β-Galactosidase

The Carbohydrate Active Enzymes database (http://www.cazy.org; Coutinho and Henrissat, 2006) includes MUM2 as a member of glycosyl hydrolase Family 35 β-galactosidases (Ahn et al., 2007). Members of this family are found in eukaryotes and prokaryotes, and there are 18 members in *Arabidopsis*. The predicted MUM2 protein has 718 amino acids, giving a predicted size of 80 kD (UniProt Version 35 identifier Q9FFN4). Identification of conserved domains using the Pfam database (Version 22.0; http://www.sanger.ac.uk/Software/Pfam; Finn et al., 2006) indicates that the MUM2 protein contains a glycosyl hydrolase catalytic domain near the N terminus as well as several PfamB domains (automatically annotated conserved domains with no assigned function) near the C terminus. Prediction of domains using the InterPro resource (version 16.0; http://www.ebi.ac.uk/interpro; Mulder et al., 2005), which searches a number of subdatabases including Pfam, Prints, SUPERFAMILY, PANTHR, and Prosite simultaneously, also reveals putative galactose binding-like domains (SUPERFAMILY version 1.69, domain ID IPR008979) that overlap with the PfamB domains predicted using the Pfam database. The predicted MUM2 protein structure

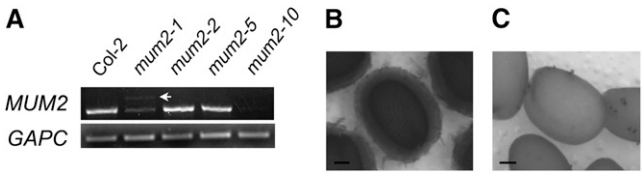

Figure 2. Transcript Analysis in *mum2* Alleles and Genomic Complementation of *mum2* with At5g63800.

(A) RT-PCR analyses on 7-DPA silique cDNA from, *mum 2-2*, *mum2-5*, and *mum2-10* using *MUM2*-specific primers. Cytosolic glyceraldehyde-3-phosphate dehydrogenase (*GAPC*) was used as a loading control. The larger product in *mum2-1* caused by inefficient splicing is indicated by an arrow.

(B) and **(C)** Ruthenium red–stained seeds. The *mum2* plants transformed with pMUM2g show complementation of the *mum2* phenotype as indicated by a restoration of wild-type mucilage extrusion **(B)**. The *mum2* plants transformed with empty pCAMBIA1200 retain a *mum2* phenotype **(C)**. Bars = 100 μm.

and the positions of the lesions in *mum2-1*, *mum2-2*, *mum2-5*, and *mum2-10* are shown in Figure 3.

An N-terminal signal peptide for secretion of the MUM2 protein was predicted using the SignalP 3.0 Server (http://www.cbs.dtu.dk/services/SignalP; Bendtsen et al., 2004). The NetNGlyc 1.0 server (http://www.cbs.dtu.dk/services/NetNGlyc) was used to identify Asn residues at positions 291 and 468 as likely sites of *N*-glycosylation (Figure 3). A possible third *N*-glycosylation site was also identified by NetNGlyc at position 538, but this was predicted to be unlikely to be glycosylated in vivo.

Detailed analysis of the catalytic mechanism has been performed for the glycosyl hydrolase Family 35 β-galactosidases from *Xanthomonas manihotis* and *Bacillus circulans*, and the catalytic nucleophile of these enzymes has been identified (Blanchard et al., 2001). Alignment of the predicted MUM2 amino acid sequence with the amino acid sequences of these bacterial enzymes using ClustalW (Chenna et al., 2003) predicts the MUM2 catalytic nucleophile to be Glu-259. The position of the catalytic proton donor has also been predicted for a human Family 35 β-galactosidase (Henrissat et al., 1995). Alignment of the predicted MUM2 protein sequence with this protein sequence using ClustalW predicts that Glu-188 is the MUM2 catalytic protein donor. The positions of these predicted catalytically active residues are shown in Figure 3.

Recombinant MUM2 Protein Is a β-Galactosidase

To determine the function of the MUM2 protein, we used the methylotrophic yeast *Pichia pastoris* to express MUM2 under the control of the methanol-inducible *AOX1* promoter. To monitor expression of MUM2 protein, we engineered a C-terminal His tag into the MUM2 protein. The parent vector and the parent vector containing the MUM2 coding sequence were introduced into yeast by homologous recombination to give stable transformants. We induced these transformants on plates containing methanol and performed filter assays to screen for expression of active MUM2 protein. The synthetic substrates used were 5-bromo-4-chloro-3-indoxyl-β-D-galactopyranoside (X-Gal) and 5-bromo-4-chloro-3-indolyl-β-D-glucuronic acid (X-Gluc). Of 25 colonies containing the MUM2 expression cassette, 23 were able to hydrolyze X-Gal and none were able to hydrolyze X-Gluc, as indicated by the blue color of free chloro-bromoindigo (data not shown). By contrast, no yeast colonies containing the empty vector were able to hydrolyze either substrate (data not shown). These results demonstrate that the recombinant MUM2 is active and has β-galactosidase activity.

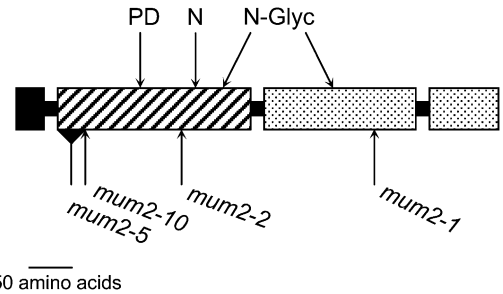

Figure 3. MUM2 Predicted Protein Structure.

The predicted MUM2 protein is 718 amino acids long. The predicted signal peptide (solid box), the glycosyl hydrolase domain (striped box), and the galactose binding-like domains (dotted box) are indicated. Arrows indicate the locations of the ethyl methanesulfonate–induced mutations in *mum2-1* (G513R) and *mum2-2* (G238E), the deletion of amino acids 62 to 93 in *mum2-5*, and the position of the T-DNA between amino acids 99 and 100 in *mum2-10*. Arrows also indicate the positions of two predicted *N*-glycosylation sites (N-glyc), the predicted catalytic nucleophile, Glu-259 (N), and the predicted catalytic proton donor, Glu-188 (PD).

We selected one colony of each genotype for further study. Initially, we performed a time course (0 to 72 h) to determine the maxima for MUM2 protein production after induction on methanol. As the pPIC9 vector used for MUM2 expression contains an α-Factor secretion signal, we monitored expression of MUM2 in the growth medium and the cell pellet by protein gel blotting using anti-His antibody. Consistent with the predicted size of the MUM2 protein, cell pellet extracts from yeast expressing MUM2 contained a His-tagged protein of ~110 kD (80 kD MUM2 plus the 30 kD α-Factor secretion signal) that was not detected in yeast transformed with the empty vector (see Supplemental Figure 2 online). MUM2 protein was not detected in the growth medium. Maximal expression of MUM2 was seen 26 h after induction.

We tested the ability of cell pellet crude extracts to hydrolyze several *p*-nitrophenyl-glycosides (PNP-glycosides; Table 1). Extracts containing recombinant MUM2, but not the control extracts, showed significant release of PNP with PNP-β-D-galactopyranoside (PNP-β-D-Gal) as substrate. We determined the activity of MUM2 for PNP-β-D-Gal to be 103 nmoles PNP h^{-1} mg^{-1} total *Pichia* protein using six independent replicates (see Supplemental Figure 2 online). Due to high nascent activity of *Pichia* extracts against PNP-β-D-glucopyranoside (PNP-β-D-Glc), the His-tagged recombinant protein was purified by batch elution from Ni^{+} resins and was shown to possess activity against PNP-β-D-Glc at 29% of activity against the galactoside. Trace activities were also detected against PNP-α- and PNP-β-L-arabinopyranosides and PNP-α-xyloside, but activities against several other PNP-glycosides were not detectable (Table 1).

The Na_2CO_3-Extractable Fraction of *mum2* Mucilage Shows Altered Monosaccharide and Linkage Composition

We used high-performance anion exchange chromatography (HPAEC) to quantify the monosaccharide composition of Na_2CO_3-extracted wild type and *mum2* mucilage after hydrolysis with sulphuric acid. These data indicate that the total monosaccharide obtained from extracted *mum2* mucilage was significantly less than that obtained from the wild type (Table 2). The amounts of the RG-I backbone sugars rhamnose (Rha) and galacturonic acid (GalA) are decreased significantly in *mum2*-extracted mucilage, while galactose (Gal) and arabinose (Ara), which are common side-chain sugars in RG-I, remain constant. In addition, *mum2*-extracted mucilage has decreased xylose (Xyl), glucose (Glc), and mannose (Man), while trace amounts of fucose (Fuc) remain constant. To examine the relative amount of each sugar in *mum2* and wild-type mucilage, the HPAEC data were also expressed as mole percentage (see Supplemental Table 1 online), highlighting the relative increase of Ara, Gal, and Glc compared with Rha and GalA in *mum2*-extracted mucilage.

Table 1. Activities against PNP-Glycosides Relative to PNP-β-D-Gal

Substrate	Relative Activity[a]
PNP-β-D-Gal	1.00
PNP-β-D-Glc	UD
PNP-α-D-galactopyranoside	ND
PNP-α-D-glucopyranoside	ND
PNP-β-D-mannopyranoside	ND
PNP-α-L-arabinofuranoside	ND
PNP-α-L-arabinopyranoside	0.01
PNP-β-L-arabinopyranoside	0.01
PNP-α-D-xylopyranoside	0.02
PNP-α-L-rhamnopyranoside	ND
PNP-α-L-rhamnofuranoside	ND

[a] Base activity against PNP-β-D-Gal was 103 nmoles PNP h^{-1} mg^{-1} total *Pichia* protein. ND, not detectable (<0.01); UD, undetermined due to high endogenous activity in *Pichia*.

Previous studies have inferred that mucilage accounts for ~60% of the Rha in whole seeds (Penfield et al., 2001; Western et al., 2001). The large differences in monosaccharide composition seen in extracted mucilage were not reflected by similar differences in composition of alcohol-insoluble residue (AIR) prepared from whole mature wild-type and *mum2* seeds without an extraction step (Table 2; Western et al., 2001). These data are also presented as mole percentage of each monosaccharide (see Supplemental Table 1 online) and indicate that there is no significant difference between *mum2* and the wild type. Therefore, these data suggest that much of the decrease in Rha and GalA observed in the extracted mucilage is due to differences in extractability from the seeds and not to decreases in the total amount of mucilage present in the seed.

As RG-I backbone residues are decreased relative to sugars typically found in RG-I side chains in *mum2* extracted mucilage, we next performed a linkage analysis to investigate structural differences in Na_2CO_3-extracted *mum2* and wild-type mucilage. Wild-type and *mum2* mucilage samples were desalted by dialysis, and uronic acids were carboxyl-reduced to their respective neutral sugars. Reduced mucilage was then per-*O*-methylated, hydrolyzed in 2 M trifluoroacetic acid (TFA), and derivitized to form partially methylated alditol acetates for quantitation of sugar linkages by gas-liquid chromatography–mass spectrometry. Data are presented as mole percentage (Table 3). Consistent with the HPAEC results, *mum2* mucilage exhibited a decrease in Rha and concomitant increases in Ara, Gal, and Glc when compared with the wild type. The mole percentage GalA is unchanged in the *mum2* mucilage.

Consistent with previous studies (Penfield et al., 2001), the predominant linkages in the mucilage of both the wild type and *mum2* are 2-linked Rha (2-Rha*p*) and 4-linked GalA (4-GalA*p*), indicating that the major polysaccharide in mucilage is RG-I (Table 3). However, in *mum2*, the amount of 2-Rha*p* is decreased by almost 50%, indicating that less RG-I backbone is extracted. In the wild type, RG-I is largely unbranched, whereas in *mum2*, an increase in branch point Rha residues (2,4-Rha*p*) were detected. Branching at the O-3 position (2,3-Rha*p*) is observed in both genotypes. The wild-type mucilage RG-I gave an unbranched: branched ratio of nearly 31:1, whereas *mum2* mucilage gave ratios less than 4:1. The percentage of 4-GalA*p* is similar between the wild type and *mum2*. Some of this (1→4)-α-linked GalA will form part of the RG-I backbone along with 2-Rha*p* and 2,4-Rha*p*, while the remainder of 4-GalA*p* likely represents HG.

Other linkages typical of neutral side chains of RG-I were identified, including (1→5)-α-arabinan with 2,5- and 3,5-Ara*f* branch point residues and type II arabinogalactan (AG-II) with (1→3)- and (1→6)-linked β-galactan chains connected in (1→3,1→6)-branch points. Very low levels of (1→4)-linked β-galactan are present, and no type I arabinogalactan (AG-I) was detected. The increased mole percentage of branch-point residues (2,4-Rha*p*) of the *mum2* RG-I correspond in part to the increases in branched (1→5)-α-arabinan as well as the nonreducing *t*-Gal*p* residues. In addition, *mum2* mucilage appears to contain increased AG-II, which may be attached to the RG-I backbone and also forms the carbohydrate moieties of arabinogalactan proteins (AGPs).

Other linkages detected indicate the presence of small amounts of other noncellulosic polysaccharides, including the *t*-GlcA*p*, 2-Xyl*p*, and 2,4-Xyl*p* of glucuronoxylans and the 4-Glc*p* and 4-Man*p* of (gluco)mannans. The small amounts of nonreducing *t*-Xyl*p* and 2-Xyl*p* compared with the presence of 4-Glc*p* and 4,6-Glc*p* indicates that xyloglucan constitutes very little of the mucilage. The glucosyl residues may be from cellulose

Table 2. Monosaccharide Composition of Mucilage Determined by HPAEC

Sugar	Wild-Type Mucilage	*mum2* Mucilage	Wild-Type Whole Seed	*mum2* Whole Seed
Fuc	0.08 ± 0.01	0.07 ± 0.01	13.65 ± 0.85	11.05 ± 0.76
Ara	0.78 ± 0.084	0.75 ± 0.1	364.25 ± 29.46	303.77 ± 17.85
Rha	23.30 ± 1.25	4.66 ± 0.52	351.26 ± 41.02	302.72 ± 25.62
Gal	1.09 ± 0.05	1.10 ± 0.12	252.01 ± 23.57	236.73 ± 19.37
Glc	3.82 ± 0.09	2.34 ± 0.15	213.73 ± 5.18	201.40 ± 7.74
Xyl	2.00 ± 0.08	0.60 ± 0.02	160.06 ± 6.56	127.54 ± 4.5
Man	0.69 ± 0.04	0.21 ± 0.03	45.38 ± 4.12	46.66 ± 1.49
GalA	33.66 ± 2.25	9.03 ± 0.52	476.02 ± 49.62	374.79 ± 47.51
Total	65.43 ± 3.71	18.73 ± 1.27	1876.37 ± 149.29	1604.65 ± 122.39

Values are the mean ± SE of four samples (mucilage) or three samples (whole seed) and are expressed as nmoles sugar normalized to milligrams of seed used for extraction (mucilage) or milligrams of AIR hydrolyzed (whole seed).

Table 3. Linkage Analysis of Wild-Type and *mum2* Mucilage

Sugar and Linkage	Wild Type	*mum2*
Fucose		
t-Fuc	tr	tr
Rhamnose		
t-Rha	0.2 ± 0	0.4 ± 0
2-Rha	49.2 ± 0.4	25.4 ± 1.9
2,3-Rha	0.4 ± 0	0.3 ± 0
2,4-Rha	1.2 ± 0	6.3 ± 0.5
Arabinose		
t-Ara*f*	0.1 ± 0	0.3 ± 0
2-Ara*f*	tr	0.2 ± 0
5-Ara*f*	0.8 ± 0	1.9 ± 0.2
2,5-Ara*f*	tr	0.6 ± 0.1
3,5-Ara*f*	tr	0.4 ± 0
Xylose		
t-Xyl*p*	0.6 ± 0	0.4 ± 0
4-Xyl*p*	2.2 ± 0.2	3.4 ± 0
2,4-Xyl*p*	0.9 ± 0	0.7 ± 0
3,4-Xyl*p*	tr	0.2 ± 0
Mannose		
t-Man*p*	ND	0.5 ± 0.1
4-Man*p*	1.3 ± 0.3	3.5 ± 0.7
Galactose		
t-Gal*p*	1.2 ± 0.1	4.3 ± 0.3
3-Gal*p*	0.4 ± 0	0.5 ± 0
4-Gal*p*	0.1 ± 0	0.3 ± 0
6-Gal*p*	ND	1.0 ± 0
3,6-Gal*p*	0.2 ± 0	0.8 ± 0
Glucose		
t-Glc*p*	tr	1.7 ± 0.4
4-Glc*p*	3.1 ± 1.0	4.5 ± 0.9
2,4-Glc*p*	0.8 ± 0.3	0.5 ± 0
3,4-Glc*p*	0.3 ± 0	0.5 ± 0
4,6-Glc*p*	0.5 ± 0.1	0.8 ± 0.1
Galacturonic Acid		
t-GalA*p*	0.3 ± 0	1.9 ± 0.1
4-GalA*p*	31.6 ± 1.2	32.9 ± 2.2
3,4-GalA*p*	1.5 ± 0.1	2.4 ± 0.2
Glucuronic acid		
t-GlcA*p*	0.3 ± 0	0.1 ± 0

Values are the mole percentage and variance of two samples (0 = <0.05). tr, trace; ND, not detected.

(4-Glc*p*) or from amylose and amylopectin, which are readily extracted by dilute alkali from underlying cell layers.

The increase in the relative proportion of *t*-Gal residues in *mum2* mucilage and in the degree of branching of RG-I are consistent with a defect in the β-galactosidase activity of the MUM2 protein.

Fourier Transform Infrared Spectroscopy Reveals Altered Polysaccharide Structures in the Na_2CO_3-Extractable Fraction of *mum2* Mucilage

Samples of Na_2CO_3-extracted *mum2* and wild-type mucilage were desalted by dialysis and freeze-dried before analysis by Fourier transform infrared (FTIR) spectroscopy. For comparison, wild-type mucilage samples were also prepared in water and freeze-dried.

Pectins give rise to peaks in the infrared spectrum at 1144, 1100, 1047, 1017, 953, 896, 857, and 835 cm^{-1}, and RG-I gives rise to peaks at 1150, 1122, 1070, 1043, 989, 951, 902, 846, and 823 cm^{-1} (Kacurácová et al., 2000). Samples extracted from wild-type seeds using water and Na_2CO_3 (see Supplemental Figure 3 online) have peaks characteristic of RG-I (1126, 1068, 1041, 987, and 821 cm^{-1}). The peaks at 1612 and 1423 cm^{-1} are carboxylate ion stretches from galacturonic acid (Kacurácová et al., 2000). Consistent with our monosaccharide analysis, this indicates that extraction with Na_2CO_3 allows the extraction of mainly pectic components from wild-type seed mucilage.

Samples of Na_2CO_3-extracted mucilage from *mum2* showed RG-I and acetylation peaks as for wild-type Na_2CO_3-extracted mucilage (peaks at 1145, 1068, 1037, 987, and 821 cm^{-1}, and 1731 and 1238 cm^{-1}, respectively). The carboxylate stretches at 1596 and 1415 cm^{-1} are shifted from 1612 and 1423 cm^{-1} and are also increased in intensity. There are also additional absorbances at 1095, 1014, 956, 898, and 860 cm^{-1} that can be assigned to pectin (see Supplemental Figure 3 online) (Kacurácová et al., 2000).

To highlight the differences between Na_2CO_3-extracted mucilage from the wild type and *mum2*, a difference spectrum representing proportional differences between the genotypes was generated by digitally subtracting an average wild-type spectrum from an average *mum2* spectrum (see Supplemental Figure 3 online). The negative peaks at 1153, 1122, 1068, 1041, and 822 cm^{-1} indicate a higher proportion of RG-I in wild-type mucilage. The positive peaks at 1577 and 1404 cm^{-1} indicate increased proportions of carboxylate ions in *mum2* mucilage. HPAEC (see Supplemental Table 1 online) and linkage analysis (Table 3) indicate that the mole percentage of Rha is decreased in *mum2* mucilage but that the 4-linked GalA content remains at wild-type levels, indicating that HG may constitute a higher proportion of Na_2CO_3-extracted *mum2* mucilage. In addition, the shift in wave number from the expected GalA absorbances of 1600 and 1420 cm^{-1} may indicate that GalA is complexed with other cell wall moieties. Positive peaks at 964, 887, and 860 cm^{-1} also indicate altered proportions of pectins in *mum2* mucilage.

MUM2 Expression Is Not Limited to the Developing Seed Coat

RT-PCR analysis using RNA extracted from developing wild-type siliques at 4, 7, 10, and 13 DPA (Figure 4A) indicated that *MUM2* transcript is present in siliques throughout development. We also detected *MUM2* transcript in roots (6 d after germination), rosette leaves, cauline leaves, stems, and open flowers (Figure 4A), suggesting that *MUM2* has biological functions additional to those in seed coat development.

The outer layer of epidermal cells in the *ap2-7* mutant does not differentiate (Western et al., 2001), making *ap2-7* a useful control to distinguish between transcripts that are expressed in the outer epidermal cells during differentiation and transcripts that are expressed in other tissues of the seed and silique. *MUM2* transcript is present in 7-DPA *ap2-7* siliques (Figure 4A), suggesting that *MUM2* is expressed in other tissues of the developing seed and silique and is not restricted to outer epidermal cells at this stage in development. As *MUM2* is expressed in *ap2*

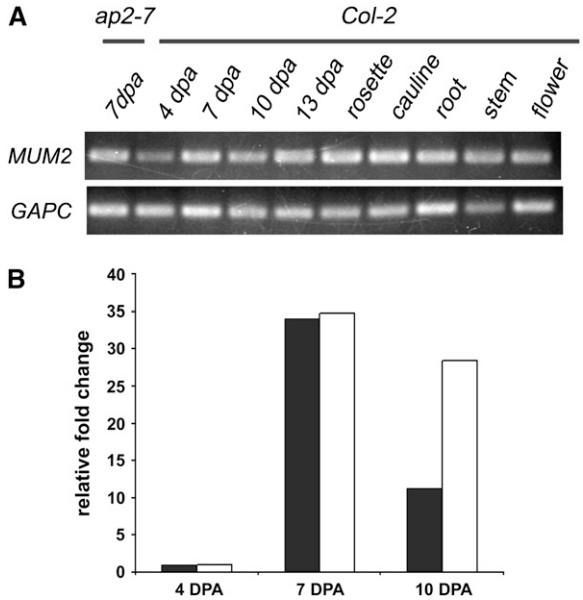

Figure 4. *MUM2* Transcript Analysis.

(A) RT-PCR analysis of MUM2 transcript in *Arabidopsis* tissues using gene-specific primers for MUM2. Cytosolic GAPC was used as a loading control. Silique RNA at 7 DPA from ap2 was used as a control for expression in seed and silique tissues other than the seed coat.

(B) Real-time PCR analysis of MUM2 transcript during seed coat development. RNA was prepared from isolated seed coats at 4, 7, and 10 DPA, and MUM2 transcript levels were determined relative to GAPC using three technical replicates. Less than 3% variation in the Ct value was seen in the technical replicates for each transcript. Data are presented as relative fold change, where the 4-DPA transcript level was set at 1.0. Two biological replicates were performed, as indicated by black and white bars.

siliques, it appears that *MUM2* is not under control of *AP2* in these tissues; however, we cannot rule out the possibility that *AP2* regulates *MUM2* expression specifically in the outer layer of the seed coat.

To examine the expression of *MUM2* more precisely, we next performed real-time PCR using RNA derived specifically from seed coats isolated from wild-type plants at 4, 7, and 10 DPA (Figure 4B). Consistent with a role in mucilage modification, these data indicate that *MUM2* is upregulated at 7 DPA when mucilage production in seed coats is at its peak.

MUM2 Protein Is Localized to the Cell Wall via the Golgi

The MUM2 protein has a predicted signal peptide for secretion to the cell wall. We constructed MUM2–green fluorescent protein (GFP) fusions under control of the 35S promoter and used them for transient expression in tobacco (*Nicotiana tabacum*). The fluorescence of MUM2-GFP was weak but could be detected in the cell wall of tobacco epidermal pavement cells, indicating that the MUM2 protein was secreted (Figure 5A). To confirm cell wall localization, tissue was stained with FM4-64 to visualize the plasma membrane. Localization of GFP external to the plasma membrane confirms that MUM2 is a secreted protein (Figure 5A, inset). Expression of the pVKH18-GFPC parent vector shows a characteristic free GFP localization pattern, with GFP present in the cytoplasm and nucleus (but not the nucleolus) (Figure 5B).

The fluorescence of GFP in the cell wall is usually weak because of the acidic pH in the apoplast (Zheng et al., 2004). We cotransformed tobacco with the MUM2-GFP fusion protein and a dominant-negative Rab1b mutant protein AtRab1b(N121I). AtRab1b is required for protein transport between the endoplasmic reticulum (ER) and the Golgi in plant cells, and the presence of AtRab1b(N121I) causes proteins that are normally secreted via the Golgi to be retained in the ER (Batoko et al., 2000). Tobacco cotransformed in this way showed an accumulation of MUM2-

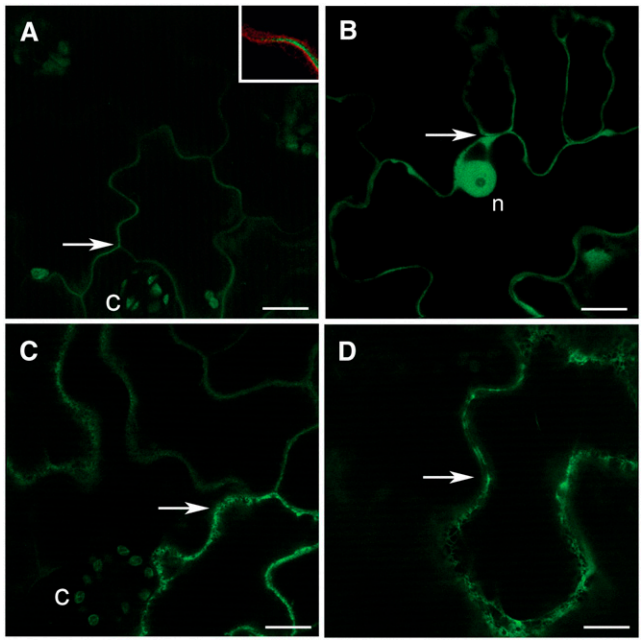

Figure 5. Localization of MUM2-GFP Fusion Protein in Tobacco Epidermal Cells.

(A) MUM2-GFP fusion protein is localized to the cell wall. Cell wall localization is characterized by a single line of fluorescence between the cells with no gaps at the corners of adjoining cells (arrow). Autofluorescence from chloroplasts in guard cells is also visible (c). To confirm this, the plasma membrane was counterstained with FM4-64 (inset, red). The pattern of staining, with the plasma membrane of adjoining cells separated by MUM2-GFP fluorescence, confirms that MUM2-GFP is located in the cell wall.

(B) Localization of free GFP in the cytosol and nucleus (n). Cytosolic localization is characterized by the lack of fluorescence in the cell walls between cells (arrow) and is distinctly different to cell wall expression (cf. **[A]** with **[B]**).

(C) MUM2-GFP coexpressed with AtRab1b(N121I) is retained in the ER. ER localization is characterized by fluorescence of the cortical network in tobacco epidermal cells (arrow). Autofluorescence from chloroplasts in guard cells is also visible (c).

(D) Expression pattern of ER-retained GFP-HDEL. Again, the cortical network characteristic of ER is evident (arrow). This expression pattern is comparable with MUM2-GFP retained in the ER (cf. **[C]** with **[D]**).

Bars = 30 μm.

GFP in a structure typical of the cortical ER (Figure 5C), as confirmed by examination of tobacco transformed with the ER-localized GFP-HDEL (Figure 5D). These data confirm that MUM2 is secreted, and its secretion to the cell wall is mediated by the Golgi.

The pVKH18-GFPC parent vector and *P35S*:MUM2-GFP constructs were introduced into *mum2* plants, and stable transformants were recovered. Seed from lines transformed with *P35S*:MUM2-GFP showed complementation of the *mum2* phenotype, indicating that the fusions were functional (see Supplemental Figure 4 online). Seed from lines transformed with pVHK18-GFPC were not complemented (see Supplemental Figure 4 online). We were unable to visualize the MUM2-GFP fusion protein in complemented plants due to a combination of dim GFP fluorescence in the apoplast caused by acidic pH (Zheng et al., 2004) and strong cell wall autofluorescence in seeds and roots.

To confirm that the MUM2-GFP fusion protein was present in the transgenic tobacco, protein gel blotting was performed using an antibody against GFP. A band of ~110 kD (79 kD corresponding to the predicted size of MUM2 plus 30 kD corresponding to GFP) was detected, indicating that the fusion protein was present and not degraded (see Supplemental Figure 4 online). We also detected full-length fusion protein in seedlings germinated from complemented seeds using protein gel blotting as described above (see Supplemental Figure 4 online).

DISCUSSION

The *MUM2* locus was identified in a screen for mutants with modified seed coat mucilage. We cloned the *MUM2* gene and identified it as a member of glycosyl hydrolase Family 35 with β-galactosidase activity. Functional MUM2-GFP protein fusions have demonstrated that the MUM2 protein is secreted to the apoplast via the ER-Golgi network. Cytological and biochemical analyses reveal that the *MUM2* gene does not greatly influence the amount of mucilage produced or the morphology of the seed coat but is required for production of mucilage with the correct structure to permit expansion when hydrated. These biochemical analyses are consistent with the β-galactosidase function of MUM2. Taken together, our data show that MUM2 functions to modify carbohydrates in the apoplast following their biosynthesis and secretion and establishes a direct link between the function of a β-galactosidase and the modification of pectin structures with specific biophysical properties. Concurrent with our investigation into the role of MUM2 in *Arabidopsis* seed coat development, complementary work conducted in the lab of Helen North corroborates the major results and conclusions of this research (Macquet et al., 2007b).

MUM2 Is Required for Expansion of Mucilage

The failure of mucilage to extrude from *mum2* seed coats could be due to a decrease in the total amount of mucilage as observed in *mum4*/*rhm2* mutants (Usadel et al., 2004; Western et al., 2004), changes in the primary cell wall that restricts mucilage expansion, or chemical alteration of the mucilage that prevents such expansion.

Our cytological data suggest that *mum2* mutants make and secrete an amount of mucilage that is comparable to the wild type. Significant decreases in total mucilage are normally associated with obvious changes in cellular morphology (Penfield et al., 2001; Western et al., 2001, 2004; Usadel et al., 2004), yet no such changes have been observed in *mum2* mutants (Figure 1). In addition, monosaccharide analysis of wild-type and *mum2* whole-seed AIR (prepared without an extraction step) reveals no major difference in the monosaccharide profiles of these two genotypes (Tables 2 and 3; Western et al., 2001). Given that much of the seed Rha and GalA appears to be derived from the mucilage (Penfield et al., 2001; Western et al., 2001), major changes in the amount of mucilage RG-I should be reflected in the total Rha observed in whole seeds, but no such decrease in Rha from whole ground seeds is apparent. These data indicate that the amount of secreted mucilage is not altered in *mum2* mutants.

MUM2 is required for production of mucilage that can be extruded on exposure of mature seeds to water (Figures 1A and 1B; Western et al., 2001). Although treatment of mature *mum2* seeds with Na_2CO_3 allows mucilage extrusion via breakage of the primary cell wall, it appears that the mucilage does not expand as much as in the wild type (Figures 1Q and 1R). Hydration of sectioned seeds also indicates that the mucilage is unable to expand even when unrestricted by the primary cell wall (Figures 1S and 1T). Although it is possible that the primary cell wall is also a target for the action of MUM2, these data indicate that MUM2 affects the hydration properties of mucilage directly. Consistent with our data indicating that *mum2* mucilage is impaired in its ability to expand, quantification of monosaccharides shows that far less total sugar is obtained from Na_2CO_3-extractable mucilage *mum2* seeds (Table 2).

Based on the data discussed here and in more detail in the following section, we propose that MUM2 is required to modify mucilage structure after secretion to produce mucilage with correct hydration properties.

MUM2 Modifies the Pectin Component of Mucilage

The chemical analyses presented here are consistent with previous studies indicating that wild-type mucilage is composed primarily of relatively unbranched RG-I (Penfield et al., 2001; Willats et al., 2001a; Western et al., 2004; Macquet et al., 2007a) and that RG-I side chains contain various neutral sugars, with arabinose and galactose as the major glycosyl residues (Ridley et al., 2001). The differences between *mum2* and wild-type mucilage involve these pectic components.

Partial extrusion of mucilage can be induced by treatment with Na_2CO_3, a chemical that has been used to extract pectin. This suggests that *mum2* mutant pectin is structurally different from the wild type. Monosaccharide analysis by HPAEC shows decreased Rha and GalA (the major sugars of the RG-I backbone) and a relative increase in side-chain sugars Gal and Ara. FTIR data also indicate that *mum2* mucilage has relatively less RG-I than the wild type and reveals relative increases in pectic components other than RG-I. A decrease in unbranched Rha accompanied by corresponding increases in the number of branch point Rha residues, arabinan side chain, and terminal

Gal residues determined by linkage analysis suggests a decrease in unbranched and an increase in branched RG-I. These data indicate that the pectic fraction and more specifically the RG-I present in Na_2CO_3-extractable *mum2* mucilage are reduced in amount and more highly branched than in the wild type. In addition, there are also increases in AG-II side chains. These may by present as part of RG-I and are also found as the carbohydrate moiety of AGPs (Vincken et al., 2003).

The altered hydration properties of *mum2* mucilage may be caused by the increased branching observed in the Na_2CO_3-extractable RG-I fraction. However, we cannot eliminate the possibility that other more subtle changes in RG-I or another component of the *mum2* mucilage, such as an increase in *mum2* seed methylation reported earlier (Western et al., 2001), are responsible for the observed changes.

Potential Targets for the MUM2 Enzyme in Mucilage

We have identified MUM2 as a member of glycosyl hydrolase Family 35 and demonstrated that it functions as a β-galactosidase. However, the in vivo target of MUM2 remains to be determined; previous studies have revealed that the substrate specificities of plant β-galactosidases can vary widely, indicating functional diversity in their activity. For example, all three isoforms of β-galactosidase isolated from ripening tomato fruit (*Solanum lycopersicum*) could hydrolyze PNP-β-D-Gal, but only one was capable of hydrolyzing the β-D-(1→4)-Gal, characteristic of galactan side chains of RG-I (Pressey, 1983). Recently, a radish (*Raphanus sativus*) β-galactosidase that showed activity toward β-D-(1→3)-Gal and β-D-(1→6)-Gal oligosaccharides and the AG-II moieties of AGPs but showed no activity toward β-D-(1→4)-Gal has been reported (Kotake et al., 2005), and the *Arabidopsis* BGAL4 protein has been shown to hydrolyze β-D-(1→3)-, β-D-(1→4)-, and β-D-(1→6)-linked galactobiosides and galactotriosides (Ahn et al., 2007). Furthermore, β-galactosidases isolated from nasturtium (*Tropaeolum majus*) cotyledons (Edwards et al., 1988) and *Copaifera langsdorffii* (de Alcantara et al., 1999) show activity toward the β-D-Gal-(1→2)-α-D-xylose side chains of xyloglucan but show little or no activity toward pectic β-D-(1→4)-Gal.

There are a number of substrates in mucilage that MUM2 may act upon, including terminal galactose (*t*-Gal), β-D-(1→4)-galactans attached to RG-I, AG-I, AG-II, and xyloglucans. However, as only low levels of β-D-(1→4)-galactans are detected in wild-type mucilage and these are not significantly altered in the mutant, and no galactosylated xyloglucans or AG-I have been observed in the wild type or mutant mucilage, the only Gal residues associated with RG-I that are available are *t*-Gal on RG-I. The linkage analysis indicates increased *t*-Gal in *mum2* mucilage, which may be the target of MUM2 activity. In addition, there are also increased AG-II residues in *mum2* mucilage, and it is not clear if these form RG-I side chains or AGP carbohydrate moieties. AGPs are implicated in a number of cellular processes, such as vegetative and reproductive growth and development, cell differentiation, and programmed cell death, but the molecular mechanisms of their actions have not been elucidated (Showalter, 2001). It has been suggested that AGPs may be involved in signaling by direct interaction with cell surface molecules (Schultz et al., 1998) or by providing a source of oligosaccharide signals (Ridley et al., 2001). Recently, it was proposed that AGPs can alter the porosity of pectins in the cell wall (Lamport et al., 2006), which may in turn affect access of modifying enzymes to pectic components. It could be envisaged that MUM2 is required to produce functional AGPs by modifying AG-II side chains.

It is also possible that MUM2 action is required as the first step in a series of modifications that together cause a more dramatic alteration in mucilage structure and properties. Such cascade effects have been documented as a feature of cell wall modification, for example, in xyloglucan breakdown during storage carbohydrate mobilization (Crombie et al., 1998) where β-galactosidase is required to carry out the first step in xyloglucan hydrolysis. The removal of galactosyl residues then allows α-xylosidase (Fanutti et al., 1991), β-glucanase (Crombie et al., 1998), and xyloglucan endotransglycosylase (Fanutti et al., 1993) to complete the hydrolysis. A similar cascade for breaking down xyloglucans has recently been identified in the *Arabidopsis* apoplast (Iglesias et al., 2006). It may also be that modification of Gal in the primary cell wall of epidermal seed coat cells is important to set the stage for other changes, such as acetylation and methylation in the mucilage itself, which causes the changes in properties of *mum2* mucilage. A model such as this, where the action of MUM2 does not directly alter the properties of mucilage but is required to process cell wall components to allow access for other cell wall modifying enzymes, may explain why there is a large change in mucilage properties upon loss of MUM2 function and may also explain the increase in arabinan RG-I side chains in *mum2* mucilage.

Cell Wall Modification by MUM2 in Other Tissues

Our results and other studies indicate that *MUM2* is expressed in all tissues examined (Iglesias et al., 2006; Macquet et al., 2007b); therefore, MUM2 may be required to play roles in wall modification elsewhere in the plant. Indeed, FTIR data available at the Purdue University Cell Wall Genomics website (http://cellwall.genomics.purdue.edu/families/index.html) indicate that *mum2-10* seedlings have an altered cell wall structure, with increased methyl esters, increased pectin, and decreased protein. It is necessary to investigate these alterations in more detail to determine the degree of similarity to the seed coat mucilage defects described here. This may provide insights into the functions of MUM2 in different tissues with potentially different substrates and interacting partners.

The Impacts of Pectin Modification on Cell Wall Properties

The structure of pectin is important in determining wall characteristics, such as mechanical properties, wall porosity, cell adhesion, and cell expansion, which in turn impact various developmental processes, such as growth, abscission, and fruit ripening. Pectin modification therefore allows the wall to fulfill different functions during the lifetime of an individual cell or in a specific tissue (Willats et al., 2001b; Knox, 2002).

One developmental process where β-galactosidase in particular has been implicated is fruit ripening. In numerous fruits, increased β-galactosidase activity is correlated with fruit ripening, and in many species, the loss of galactose and arabinose

from the wall is associated with fruit softening and an increase in pectin solubility (for a review, see Brummell, 2006). Although the mechanisms by which β-galactosidases are involved in cell wall modifications are not entirely clear, a functional role for β-galactosidases that alter wall properties during fruit ripening has been demonstrated. For example, the carambola β-galactosidase from ripe fruit is active against various galactans and can depolymerize structurally intact pectin and modify hemicelluloses (Balasubramaniam et al., 2005), and papaya β-galactosidase from ripe fruit has been shown to be capable of hydrolyzing cell wall components in unripe fruit (Lazan et al., 2004). It may be that there are analogies between fruit ripening and mucilage modification in the seed coat.

Establishing a relationship between pectin structure and function can be difficult, and predicting the effects of altering pectin structure is not trivial. The spatial and temporal distribution of epitopes in the wall is likely to be important in determining pectin properties, as are interactions between both pectins themselves and other cell wall components, such as hemicellulose and cellulose (Vincken et al., 2003). Our data show that the seed coat model system can be used to identify enzymes that are involved in cell wall modification and that impact the physical and biochemical properties of cell walls. Further investigation into the pectin modifications in mucilage and into cell wall modifications in other tissues in *mum2* mutants may further improve our understanding of this structure-function relationship. The mechanism by which MUM2, a β-galactosidase whose function is to remove terminal galactose residues from polysaccharides, can alter the hydration properties of mucilage so radically remains a key question. In particular, the identification of the in vivo substrate of MUM2 should provide insights into how modification of cell wall architecture can have a dramatic effect on wall properties.

METHODS

Plant Material and Growth Conditions

mum2-1 (Western et al., 2001), *mum2-2*, and *mum2-9* were isolated from an ethyl methanesulfonate–mutagenized M3 population of wild-type Col-2 *Arabidopsis thaliana* plants: *mum2-3* and *mum2-4*/*scm4* are T-DNA insertion lines in the Ws-2 background isolated from the Feldman collection (gift from Scott Sattler and David Marks, University of Minnesota); *mum2-5*, *mum2-6*, and *mum2-7* are Fast Neutron lines in a Col-0 background carrying a *gl1* mutation; *mum2-8* is a Fast Neutron line in Col-0; *mum2-10* (SALK_011436; Alonso et al., 2003) is a T-DNA insertion line in the Col-0 background obtained from the ABRC. Alleles are available from ABRC through TAIR (www.arabidopsis.org).

Seeds were germinated on AT minimal medium (Haughn and Somerville, 1986) in growth chambers at 20°C under continuous light (90 to 120 μmol $m^{-2}s^{-1}$ PAR) and then transferred at 7 to 10 d after germination to prepared soil mix (Sunshine Mix 5; Sun Gro Horticulture), watered with liquid AT medium, and grown under the same conditions as above.

For staging of siliques, open flowers 0 DPA were marked with nontoxic, water-soluble paint to allow the selection of developing siliques at precise ages.

Microscopy

Whole seeds were stained by shaking in 0.01% (w/v) Ruthenium Red (Sigma-Aldrich) for 2 h and then mounted in water and viewed using a dissecting microscope. To investigate release of mucilage by Ca^{2+} chelators, alkali, and guanidine thiocyanate, seeds were shaken for 2 h in the chelator, alkali, or guanidine solution at room temperature, rinsed twice with water, and then stained with Ruthenium Red, as described above.

For resin embedding and sectioning, developing seeds were fixed with 3% (v/v) glutaraldehyde (Canemco) in 0.5 M sodium phosphate, pH 7. Postfixation with 1% (v/v) osmium tetraoxide, dehydration, embedding, and sectioning were as described by Western et al. (2000). Thick sections (0.2 to 0.5 μm) were stained with 1% (w/v) Toluidine Blue O in 1% (w/v) sodium borate, pH 11, and photographed using a Zeiss AxioScop light microscope (Carl Zeiss).

Mature unfixed seeds were prepared for sectioning by embedding in Paraplast (Sigma-Aldrich). Seeds were added to molten Paraplast medium and then incubated at 60°C for 2 h before hardening overnight at ambient temperature. Sections approximately one cell's width (20 μm thick) were prepared and hydrated with 0.01% (w/v) Ruthenium Red and then imaged as described above.

Samples were dry-mounted on stubs, coated with gold-palladium in a SEMPrep2 sputter coater (Nanotech), and imaged using a Hitachi S4700 scanning electron microscope (Hitachi High-Technologies Canada).

Digital photographs were manipulated with Adobe Photoshop (Adobe Photosystems) to prepare figures.

Positional Cloning of *MUM2*

A mapping population of 2016 F2 plants was generated from a cross between *mum2-1* (Col-2 background) and wild-type Landsberg *erecta* plants. Simple sequence length polymorphisms were identified using sequence information available from the Arabidopsis Genome Initiative (2000) and Cereon (Jander et al., 2002). Primer sequences are available at TAIR (www.arabidopsis.org).

SALK_011436 was genotyped by PCR using gene-specific primers (At5g63800 F5, 5′-GCAAACGATTCTCTCCTTGG-3′; At5g63800 R5, 5′-CCATGTAAGCTCCAGAGTGG-3′) and a primer to the left border of the T-DNA insertion (LBb1, 5′-GCGTGGACCGCTTGCTGCAACT-3′).

Molecular complementation of *mum2-1* was performed using a PCR fragment amplified from BAC MKB5 (At5g63800compF *Sac*I, 5′-GTACTTCACGGTGTAGCAGC-3′, and At5g63800compR *Kpn*I, 5′-ATATCTGCAGATCCTGATCCTCTCACCACG-3′). The fragment was cloned into pCAMBIA1200 (http://www.cambia.org/daisy/cambia/home.html) to give pMUM2g. As the inserts were not sequenced, four independent clones were selected for transformation. *mum2-1* plants were transformed with either pMUM2g or pCAMBIA1200 by the *Agrobacterium tumefaciens* dipping method (Clough and Bent, 1998) using strain LBA4404 (Hoekema et al., 1983). Hygromycin-resistant plants were identified by growth of T1 plants on AT medium supplemented with 25 μg/mL hygromycin B (Invitrogen Life Technologies).

Heterologous Expression of MUM2 in *Pichia pastoris* and Determination of MUM2 Enzyme Activity

The MUM2 coding sequence without the endogenous signal peptide was cloned into the pPIC9 vector supplied with the Invitrogen *Pichia* expression kit by PCR using the primers pPIC9F (5′-ATCTCGAGAAAAGAGAGGCTGAAGCTGCGAAGGGAGTAACGTACGACGGACGG-3′) and pPIC9R+His (5′-GCTAGCGGCCGCTCAATGATGATGATGATGATGGGAGAATTGAGATTGAGCTTGACTCGA-3′). *Pichia* strain GS115 was transformed with the finished construct and the parent pPIC9 vector by electroporation, and pure clonal isolates were obtained according the kit instructions. Transformed yeast colonies were maintained on MD plates (1.34% yeast nitrogen base without amino acids, 4×10^{-5}% biotin, 2% dextrose, and 15 g/L agar). For induction, cultures were grown in MD liquid medium before induction was performed in MM liquid medium

(1.34% yeast nitrogen base without amino acids, 4×10^{-5}% biotin, and 1% methanol). For filter assays, induction was performed on MM plates (MM liquid medium plus 15 g/L agar).

Filter assays were prepared by transferring yeast colonies onto nitrocellulose membranes that were then flash-frozen in liquid nitrogen to permeabilize the yeast cells. Filters were then incubated at 37°C in 50 mM sodium acetate buffer, pH 5.0, containing 2 mM X-Gal or X-Gluc.

Protein samples from supernatants after cell culture were prepared by trichloroacetic acid precipitation. Protein samples from cell pellets for protein gel blots were prepared using yeast protein extraction reagent (Y-PER; Pierce Biotechnology) according to the manufacturer's instructions. Five microliters of the resulting supernatant was separated by SDS-PAGE on a 10% gel (Laemmli, 1970) and transferred to nitrocellulose membrane by semidry electroblotting. Penta-His antibody (Qiagen) and whole molecule anti-Mouse IgG–Alkaline Phosphatase conjugate (Sigma-Aldrich) were used as directed by the manufacturer and developed using NBT/BCIP (Roche).

Cell pellets for enzyme assays were stored at −80°C until required. Pellets were thawed on ice and resuspended in 2 mL of 50 mM sodium acetate, pH 5.0, per 100 mL of induced culture. Cells were disrupted using glass beads and a bead beater according to standard protocols. The cell debris was removed, and the supernatant cleared by two successive centrifugations at 14,000 rpm for 10 min at 4°C. Protein in the resulting extracts was determined using protein assay reagent (Bio-Rad) according to the manufacturer's instructions, and 50 mM sodium acetate, pH 5.0, was added if necessary to equalize the protein concentrations in extracts from different genotypes. Protein extract (100 μL) and 24 μL of 10 mM PNP-glycoside were incubated at 37°C for 20 h before the reaction was stopped by the addition of 60 μL of 1 M sodium carbonate. PNP release was determined by measuring absorption at 405 nm. Standard curves for PNP were prepared to allow conversion of absorption to μmoles PNP. Controls consisting of boiled extracts from both genotypes were used to correct for background hydrolysis of PNP-glycoside during the assay. Low amounts of activity were seen in extracts containing the empty pPIC9 vector, and these were used to correct for endogenous activity. All samples were prepared in duplicate.

Other than PNP-β-D-glucoside, reactions against all substrates were negligible in the control *Pichia* extracts containing the empty pPIC9 vector. However, because of a high background activity against the β-D-glucoside in the *Pichia* extracts, this activity relative to that against PNP-β-D-galactoside was determined after purification of the His-tagged recombinant protein on Ni^{+} resin. Four milliliters each of the *Pichia* control and MUM2 extracts in ice-cold 20 mM imidazole[HEPES], pH 7.4, containing 0.5 M NaCl was added to a 200-μL suspension of the Ni^{+} resin (Ni Sepharose 6 Fast-Flow; Amersham) and incubated on a rocking shaker for 1 h. The resin was washed with three times with 15 mL each of the loading buffer and then three times with 15 mL each of 50 mM imidazole[HEPES], pH 7.4, containing 1.0 M NaCl, and then the proteins eluted with 1.5 mL of 300 mM imidazole[HEPES], pH 7.4, containing 1.0 M NaCl. To change buffers, the eluate was passed through a Sephadex G-25 desalting column (PD-10; GE Healthcare) equilibrated in 50 mM sodium acetate, pH 5.0. The protein fraction devoid of imidazole was collected and used in the assay directly. No protein was detected from the control extracts, but the same elution volumes were collected and used in the assays. No activities against either PNP-β-D-galactoside or PNP-β-D-glucoside were detected in the control reactions.

Extraction of Mucilage with Na_2CO_3

Approximately 30 mg of seed (exact weight recorded) was mixed with 0.7 mL of 1 M Na_2CO_3, and the seeds were shaken on an orbital shaker for 20 min to facilitate wetting. The supernatant (0.5 mL) was removed and retained as a mucilage fraction, 0.7 mL of water was added to the seeds, and they were shaken for a further 2 h using a vortex mixer on medium speed. Half a milliliter of this supernatant was removed and pooled with the 0.5 mL of supernatant in 1 M Na_2CO_3, giving 1 mL of mucilage in ~0.5 M Na_2CO_3. Samples were desalted by dialysis using 100 D cutoff cellulose ester membrane (Spectra/Por Biotech; Spectrum Labs) for 30 h in 0.05% chlorobutol in water to prevent microbial growth. Dialysate was changed three to four times during this period.

Determination of Monosaccharide Composition by HPAEC

To prepare mucilage samples for HPAEC, ~30 mg of seeds (exact weight recorded) were mixed with 50 μL of 1 M sodium carbonate and left to stand at room temperature for 20 min before 1.2 mL of water and 10 μL of 5 mg/mL D-erythritol was added as an internal standard and the samples vortexed for 2 h on medium speed. Samples were then dried at 60°C under a stream of nitrogen. Sulphuric acid (72%, 20.25 μL) was added to each sample, and they were incubated on ice for 2 h. Water (480 μL) was then added to give a final concentration of 4% sulphuric acid, and the samples were autoclaved for 60 min at 121°C before being filtered through 0.45-μm nylon syringe filters.

To prepare AIR, whole seeds (~15 mg) were ground to a fine powder by mortar and pestle in liquid nitrogen. The powders were suspended in 1 mL of 70% (w/v) ethanol and heated at 60°C for 10 min to inactivate enzymes. Three 30-min washes in 1 mL 70% ethanol with shaking were then performed to remove small soluble sugars. The AIR fractions were collected by centrifugation in a microcentrifuge between washes. The AIR was dried under nitrogen and weighed before 10 μL of 5 mg/mL D-erythritol was added. Two to five milligrams of AIR was hydrolyzed using sulphuric acid as described above.

Neutral sugar standards (fucose, arabinose, rhamnose, galactose, glucose, mannose, and xylose) and acid sugar standards (galacturonic acid), prepared with and without sodium carbonate as required, were also processed in this way.

The identity and concentration of neutral monosaccharide sugars was determined using HPAEC analysis on a DX-600 BioLC chromatograph (Dionex). Separation was achieved on a CarboPac PA1 anion exchange column (Dionex), and detection was achieved via pulsed amperometry across a gold electrode. A 20-μL volume of sample was injected. The column was equilibrated with 250 mM NaOH and eluted with deionized water at a flow rate of 1.0 mL min^{-1}. Detection of carbohydrates was facilitated with a postcolumn addition of 200 mM NaOH at 0.5 mL min^{-1}. The concentration of acid sugars in the filtrate was determined with the identical HPLC system and column, with a different elution gradient: sugars were eluted in 100 mM NaOH with a linear gradient (curve 5) of 0 to 400 mM sodium acetate from 5 to 40 min, followed by a 10 min 300 mM NaOH wash. The column was then equilibrated to 100 mM NaOH prior to the next injection.

Monosaccharides were quantified with the D-erythritol internal standard after correction of response factors with monosaccharide standards of different concentrations to allow area to be converted to molar amounts. Sugars from mucilage were normalized to the mass of seed extracted, and sugars from whole-seed AIR were normalized to the mass of AIR.

Carbohydrate Linkage Analysis

Dialyzed mucilage samples extracted with Na_2CO_3 were used for carbohydrate linkage analysis. The uronosyl groups in mucilage polysaccharides were carboxyl reduced with sodium borodeuteride after activation with a water-soluble diimide (Carpita and McCann, 1996). The sample was then divided, with half of it was used for determination of monosaccharide composition and the other half used for linkage analysis (see below). For monosaccharide composition, mucilage was hydrolyzed with 2 M TFA containing 1 μmol of myo-inositol (internal standard) for 90 min at

120°C. The TFA was evaporated under a stream of nitrogen, and the sugars were converted to alditol acetates (Gibeaut and Carpita, 1991). The alditol acetates were separated by gas–liquid chromatography on a 0.25 mm × 30 m vitreous silica capillary column of SP-2330 (Supelco). Temperature was programmed from an initial 80°C hold for 1 min during injection, to 170°C at 25°C/min, and then to 240°C at 5°C/min with a 6-min hold at the upper temperature. The proportion of galacturonic acid was determined as the proportion of 6,6-dideuterogalactose in total galactose by electron-impact mass spectrometry according to the equation described by Kim and Carpita (1992), which accounts for ^{13}C spillover.

For determination of sugar linkages within the mucilage, the second portion of the carboxyl-reduced mucilage samples were per-*O*-methylated with Li^+ methylsulfinylmethanide and methyl iodide according to Gibeaut and Carpita (1991). The per-*O*-methylated polymers were recovered after addition of water to the mixture and partitioning into chloroform. The chloroform extracts were washed five times with at least threefold excess of water, and the chloroform was evaporated under a stream of nitrogen. The methylated polymers purified by chloroform partitioning were hydrolyzed in 2 M TFA for 90 min at 120°C. The sugars were then reduced with $NaBD_4$ and acetylated. The partly methylated alditol acetates were separated by gas–liquid chromatography on a 0.25 mm × 30 m vitreous silica capillary column of SP-2330 (Supelco). Temperature was programmed from an initial 80°C hold for 1 min during injection, to 160°C at 25°C/min, then to 210°C at 2°C/min, and then to 240°C at 5°C/min, with a 6-min hold at the upper temperature. All linkages were deduced by a combination of retention time and electron-impact mass spectrometry of the derivatives (Carpita and Shea, 1989).

FTIR Spectroscopy

Na_2CO_3-extracted dialyzed mucilage samples were freeze-dried then dissolved in water (1 mg/mL). Ten microliters were air-dried in the wells of IR-reflective, gold-plated microscope slides (Thermo-Electron) and supported on the stage of a Nicolet Continuum series microscope accessory to a 670 IR spectrophotometer with a liquid nitrogen–cooled mercury-cadium telluride detector (Thermo-Electron). An area of sample (up to 125 × 125 μm) was selected for spectral collection in transflectance mode. One hundred and twenty-eight interferograms collected with 8 cm^{-1} resolution were co-added to improve the signal-to-noise ratio for each sample. For mucilage samples, 30 spectra were collected, and each was area averaged and baseline corrected prior to generating average spectra and digital subtraction spectra as described previously (Chen et al., 1998).

RT-PCR

RNA was isolated from plant tissue as described by Western et al. (2004). RNA was treated with DNaseI (Invitrogen) and reverse transcribed with SuperScript II reverse transcriptase (Invitrogen) according to the manufacturer's instructions.

The complete *MUM2* cDNA including 5′ and 3′ untranslated regions was amplified with At5g63800 F9 (5′-TCTCAAATCTCAAATCTCAAA-3′) and At5g63800 R6 (5′-GAAGTTTCTTTACATGTGACAC-3′).

For RT-PCR under nonsaturating conditions, gene-specific primers surrounding an intron were designed for *MUM2* (At5g63800 F5, 5′-GCAAACGATTCTCTCCTTGG-3′, and At5g63800 R5, 5′-CCATGTAAGCTCCAGAGTCC-3′) and *GAPC* (GAPC P1, 5′-TCAGACTCGAGAAAGCTGCTAC-3′, and GAPC P2, 5′-GATCAAGTCGACCACACGG-3′; Western et al., 2004). The number of PCR cycles required for amplification in the linear range was determined for *GAPC* (23 cycles) and *MUM2* (35 cycles). Amplification of *GAPC* was used as a loading control for *MUM2* RT-PCRs. RT-PCR was performed a minimum of three times using each set of primers to confirm results.

Real-Time PCR

Total RNA was extracted from 4-, 7-, and 10-DPA Col-2 seed coats using the RNAqueous kit (Ambion), and cDNA was synthesized using SuperScript III RNA polymerase (Invitrogen). Amplification was performed using the MJ mini opticon real-time PCR system (Bio-Rad) with *GAPC* as the internal control. The following gene-specific primers were used: GAPCp1, 5′-TCAGACTCGAGAAAGCTGCTAC-3′; GAPCp2, 5′-GATCAAGTCGACCACACGG-3′; MUM2p1, 5′-GTTACAACGCCGGTTCAAGT-3′; MUM2p2, 5′-ACGTGGACAACATGTCCTGA-3′. Each 20-μL reaction contained 10 μL of SYBR Green Supermix reagent (Bio-Rad), 1 μL of cDNA, and 0.2 mM each primer. Reactions were performed in triplicate. PCR conditions were 95°C for 3 min and then 40 cycles of 95°C for 10 s, 54°C for 30 s, and 72°C for 30 s. Data were analyzed using Gene Expression Macro software (version 1.1; Bio-Rad).

Subcellular Localization of MUM2 Protein

To generate GFP-fused MUM2, the vector pVKH18-GFPC was first constructed using the following steps. The coding sequence of GFP5 in pVKH18-GFP-HDEL (Batoko et al., 2000) was amplified with primers GFP5C5 (5′-CG*GGATCC*GCC*GTCGAC*ATGAGTAAAGGAGAAGAACTTTTCACTGG-3′) and GFP5C3 (5′-CG*GGATCCGAGCTC*TTATTTGTATAGTTCATCCATGCCATGTG-3′) and subcloned into pBlueScript KS as a *Bam*HI-*Bam*HI fragment. The subcloned GFP was sequenced and used as a *Bam*HI-*Sac*I fragment to replace secGFP in pVKH18-sGFP (Batoko et al., 2000) to create pVKH18-GFPC. The cDNA of the *MUM2* gene was then subcloned into pVKH18-GFPC to produce the C-terminal MUM2-GFP fusion under the control of the cauliflower mosaic virus 35S promoter. Due to the presence of a putative ER targeting signal peptide in MUM2, only C-terminal GFP fusion was constructed. pVKH18 carrying the MUM2-GFP fusion was named *P35S*:MUM2-GFP. The generation of *P35S*:GFP-HDEL and *P35S*:*At*Rab1b(N121I) is described by Batoko et al. (2000).

pVHK18-GFPC, *P35S*:MUM2-GFP, *P35S*:*At*Rab1b(N121I), and *P35S*:GFP-HDEL constructs were introduced transiently into tobacco (*Nicotiana tabacum*) according to the method of Batoko et al. (2000) with the modification that the infiltration buffer consisted of 50 mM MES, pH 5.6, 10 mM $MgCl_2$, and 150 μM acetosyringone (Sigma-Aldrich). Transiently transformed tobacco leaf discs were incubated in 8.2 μM FM4-64 dye (Molecular Probes, Invitrogen Life Technologies) for 1 h to allow visualization of the plasma membrane.

Confocal imaging of samples mounted in water was performed according to Zheng et al. (2005) using a Bio-Rad Radiance Plus on an inverted Zeiss Axiovert (Carl Zeiss). ImageJ software (http://rsb.info.nih.gov/ij/) and Adobe Photoshop (Adobe Photosystems) were used for post-acquisition image processing.

The *mum2-1* plants were transformed with either pVKH18-GFPC or *P35S*:MUM2-GFP as described above. To confirm the presence of full-length MUM2-GFP protein fusion in plants, protein samples were prepared by grinding tissue in 2× SDS loading buffer, boiling for 10 min, and then centrifuging to remove cell debris. Protein gel blotting was performed as described above using polyclonal anti-GFP (IgG fraction from rabbit; Molecular Probes, Invitrogen Life Technologies) and whole molecule anti-Rabbit IgG-alkaline phosphatase conjugate (Sigma-Aldrich).

Accession Numbers

Sequence data from this article can be found in the GenBank/EMBL data libraries under accession numbers NM_125775 and Q9FFN4 (At5g63800; *MUM2*), P16278 (human β-galactosidase), BAA21669 (*Bacillus circulans* β-galactosidase), and P48982 (*Xanthomonas manihotis* β-galactosidase).

Supplemental Data

The following materials are available in the online version of this article.

Supplemental Figure 1. Extraction of Mucilage from *mum2* Seeds Using Chelating Agents.

Supplemental Figure 2. Heterologous MUM2 Expression in *Pichia pastoris*.

Supplemental Figure 3. FTIR Spectroscopy Analysis of Wild-Type and *mum2*-Extracted Mucilage Extracted with Water and Na_2CO_3.

Supplemental Figure 4. Complementation of *mum2* with *P35S*: MUM2-GFP.

Supplemental Table 1. Monosaccharide Composition of Mucilage Determined by HPAEC Expressed as Mole Percentage of Each Monosaccharide.

ACKNOWLEDGMENTS

We thank Scott Sattler and David Marks for sharing the *mum2-3* and *mum2-4*/*scm2* alleles; Chris Somerville, Steve Withers, Owen Rowland, and Andy Dean for comments and discussion; and Xin Li and Geoff Wasteneys for critical reading of the manuscript. We also thank the staff at the University of British Columbia BioImaging facility for invaluable help with microscopy. This work was supported by a Natural Science and Engineering Research Council of Canada Discovery grant and a Designing Oilseeds For Tomorrow's Markets, Genome Alberta/Genome Canada grant to G.W.H. N.C.C. and M.C.M. acknowledge support of Grant DBI-0217552 from the National Science Foundation Plant Genome Research Program. M.C.M. acknowledges support of U.S. Department of Energy Grant DE-FG02-03ER15445.

Received January 22, 2007; revised December 10, 2007; accepted December 12, 2007; published December 28, 2007.

REFERENCES

Ahn, Y.O., Zheng, M., Bevan, D.R., Esen, A., Shiu, S.H., Benson, J., Peng, H.P., Miller, J.T., Cheng, C.L., Poulton, J.E., Shih, M.C. (2007). Functional genomic analysis of *Arabidopsis thaliana* glycoside hydrolase family 35. Phytochemistry **68:** 1510–1520.

Alonso, J.M., et al. (2003). Genome-wide insertional mutagenesis of *Arabidopsis thaliana.* Science **301:** 653–657.

Arabidopsis Genome Initiative (2000). Analysis of the genome sequence of the flowering plant *Arabidopsis thaliana.* Nature **408:** 796–815.

Balasubramaniam, S., Lee, H.C., Lazan, H., Othman, R., and Ali, Z.M. (2005). Purification and properties of a β-galactosidase from carambola fruit with significant activity towards cell wall polysaccharides. Phytochemistry **66:** 153–163.

Batoko, H., Zheng, H.Q., Hawes, C., and Moore, I. (2000). A Rab1 GTPase is required for transport between the endoplasmic reticulum and Golgi apparatus and for normal Golgi movement in plants. Plant Cell **12:** 2201–2217.

Beeckman, T., De Rycke, R., Viane, R., and Inzé, D. (2000). Histological study of seed coat development in *Arabidopsis thaliana.* J. Plant Res. **V113:** 139–148.

Bendtsen, J.D., Nielsen, H., von Heijne, G., and Brunak, S. (2004). Improved prediction of signal peptides: SignalP 3.0. J. Mol. Biol. **340:** 783–795.

Blanchard, J.E., Gal, L., He, S., Foisy, J., Warren, R.A., and Withers, S.G. (2001). The identification of the catalytic nucleophiles of two β-galactosidases from glycoside hydrolase family 35. Carbohydr. Res. **333:** 7–17.

Brummell, D.A. (2006). Cell wall disassembly in ripening fruit. Funct. Plant Biol. **33:** 103–119.

Carpita, N.C., and McCann, M.C. (1996). Some new methods to study plant polyuronic acids and their esters. In Progress in Glycobiology, R. Townsend and A. Hotchkiss, eds (New York: Marcel Dekker), pp. 595–611.

Carpita, N.C., and Shea, D. (1989). Linkage structure of carbohydrates by gas chromatograph-mass spectrometry (GC-MS) of partially methylated alditol acetates. In Analysis of Carbohydrates by GLC and MS, C.J. Biermann and G.D. McGinnis, eds (Boca Raton, FL: CRC Press), pp. 155–216.

Chen, L., Carpita, N.C., Reiter, W.D., Wilson, R.H., Jeffries, C., and McCann, M.C. (1998). A rapid method to screen for cell-wall mutants using discriminant analysis of Fourier transform infrared spectra. Plant J. **16:** 385–392.

Chenna, R., Sugawara, H., Koike, T., Lopez, R., Gibson, T.J., Higgins, D.G., and Thompson, J.D. (2003). Multiple sequence alignment with the Clustal series of programs. Nucleic Acids Res. **31:** 3497–3500.

Clough, S.J., and Bent, A.F. (1998). Floral dip: A simplified method for *Agrobacterium*-mediated transformation of *Arabidopsis thaliana.* Plant J. **16:** 735–743.

Coutinho, P.M., and Henrissat, B. (2006). Carbohydrate-active enzymes: An integrated database approach. In Recent Advances in Carbohydrate Bioengineering, H.J. Gilbert, G. Davies, B. Henrissat, and B. Svensson, eds (Cambridge, UK: Royal Society of Chemistry), pp. 3–12.

Crombie, H.J., Chengappa, S., Hellyer, A., and Reid, J.S.G. (1998). A xyloglucan oligosaccharide-active, transglycosylating-D-glucosidase from the cotyledons of nasturtium (*Tropaeolum majus* L.) seedlings - Purification, properties and characterization of a cDNA clone. Plant J. **15:** 27–38.

de Alcantara, P.H.N., Dietrich, S.M.C., and Buckeridge, M.S. (1999). Xyloglucan mobilisation and purification of a (XLLG/XLXG) specific β-galactosidase from cotyledons of *Copaifera langsdorffii.* Plant Physiol. Biochem. **37:** 653–663.

Edwards, M., Bowman, Y.J., Dea, I.C., and Reid, J.S. (1988). A β-D-galactosidase from nasturtium (*Tropaeolum majus* L.) cotyledons. Purification, properties, and demonstration that xyloglucan is the natural substrate. J. Biol. Chem. **263:** 4333–4337.

Fanutti, C., Gidley, M.J., and Reid, G.J.S. (1991). A xyloglucan-oligosaccharide-specific α-D-xylosidase or *exo*-oligoxyloglucan-α-xylohydrolase from germinated nasturtium (*Tropaeolum majus* L.) seeds. Planta **184:** 137–147.

Fanutti, C., Gidley, M.J., and Reid, J.S.G. (1993). Action of a pure xyloglucan *endo*-transglycosylase (formerly called xyloglucan-specific *endo*-(1→4)-beta-D-glucanase) from the cotyledons of germinated nasturtium seeds. Plant J. **3:** 691–700.

Finn, R.D., et al. (2006). Pfam: Clans, web tools and services. Nucleic Acids Res. **34:** D247–D251.

Fry, S.C. (2000). The Growing Plant Cell Wall: Chemical and Metabolic Analysis. (Caldwell, NJ: The Blackburn Press).

Gibeaut, D.M., and Carpita, N.C. (1991). Cleanup procedure for partially methylated alditol acetate derivatives of polysaccharides. J. Chromatogr. **587:** 284–287.

Hanke, D.E., and Northcote, D.H. (1975). Molecular visualisation of pectin and DNA by ruthenium red. Biopolymers **14:** 1–17.

Haughn, G., and Chaudhury, A. (2005). Genetic analysis of seed coat development in *Arabidopsis.* Trends Plant Sci. **10:** 472–477.

Haughn, G.W., and Somerville, C. (1986). Sulfonylurea-resistant mutants of *Arabidopsis thaliana.* Mol. Gen. Genet. **204:** 430–434.

Henrissat, B., Callebaut, I., Fabrega, S., Lehn, P., Mornon, J.-P., and Davies, G. (1995). Conserved catalytic machinery and the prediction of a common fold for several families of glycosyl hydrolases. Proc. Natl. Acad. Sci. USA **92:** 7090–7094.

Hoekema, A., Hirsch, P.R., Hooykaas, P.J.J., and Schilperoort, R.A. (1983). A binary plant vector strategy based on separation of vir- and T-region of the *Agrobacterium tumefaciens* Ti-plasmid. Nature **303:** 179–180.

Iglesias, N., Abelenda, J.A., Rodiño, M., Sampedro, J., Revilla, G., and Zarra, I. (2006). Apoplastic glycosidases active against xyloglucan oligosaccharides of *Arabidopsis thaliana.* Plant Cell Physiol. **47:** 55–63.

Jander, G., Norris, S.R., Rounsley, S.D., Bush, D.F., Levin, I.M., and Last, R.L. (2002). Arabidopsis map-based cloning in the post-genome era. Plant Physiol. **129:** 440–450.

Kacurácová, M., Capek, P., Sasinková, V., Wellner, N., and Ebringerová, A. (2000). FT-IR study of plant cell wall model compounds: Pectic polysaccharides and hemicelluloses. Carbohydr Polym. **43:** 195–203.

Kim, J.B., and Carpita, N.C. (1992). Changes in esterification of the uronic-acid groups of cell-wall polysaccharides during elongation of maize coleoptiles. Plant Physiol. **98:** 646–653.

Knox, J.P. (2002). Cell and developmental biology of pectins. In Pectins and Their Manipulation, G.B. Seymour and J.P. Knox, eds (Boca Raton, FL: CRC Press), pp. 131–149.

Kotake, T., Dina, S., Konishi, T., Kaneko, S., Igarashi, K., Samejima, M., Watanabe, Y., Kimura, K., and Tsumuraya, Y. (2005). Molecular cloning of a β-galactosidase from radish that specifically hydrolyzes β-(1→3)- and β-(1→6)-galactosyl residues of arabinogalactan protein. Plant Physiol. **138:** 1563–1576.

Laemmli, U.K. (1970). Cleavage of structural proteins during the assembly of the head of bacteriophage T4. Nature **227:** 680–685.

Lamport, D.T.A., Kieliszewski, M.J., and Showalter, A.M. (2006). Salt stress upregulates periplasmic arabinogalactan proteins: Using salt stress to analyse AGP function. New Phytol. **169:** 479–492.

Lazan, H., Ng, S.Y., Goh, L.Y., and Ali, Z.M. (2004). Papaya β-galactosidase/galactanase isoforms in differential cell wall hydrolysis and fruit softening during ripening. Plant Physiol. Biochem. **42:** 847–853.

Macquet, A., Ralet, M.C., Kronenberger, J., Marion-Poll, A., and North, H.M. (2007a). In-situ, chemical and macromolecular study of the composition of *Arabidopsis thaliana* seed coat mucilage. Plant Cell Physiol. **48:** 984–999.

Macquet, A., Ralet, M.-C., Loudet, O., Kronenberger, J., Mouille, G., Marion-Poll, A., and North, H.M. (2007b). A naturally occurring mutation in an *Arabidopsis* accession affects a β-D-galactosidase that increases the hydrophilic potential of rhamnogalacturonan I in seed mucilage. Plant Cell **19:** 3990–4006.

McCartney, L., and Knox, J.P. (2002). Regulation of pectic polysaccharide domains in relation to cell development and cell properties in the pea testa. J. Exp. Bot. **53:** 707–713.

Mulder, N.J., et al. (2005). InterPro, progress and status in 2005. Nucleic Acids Res. **33:** D201–D205.

O'Neill, M.A., and York, W.S. (2003). The composition and structure of plant primary cell walls. In The Plant Cell Wall, J.K.C. Rose, ed (Boca Raton, FL: CRC Press), pp. 1–54.

Penfield, S., Meissner, R.C., Shoue, D.A., Carpita, N.C., and Bevan, M.W. (2001). *MYB61* is required for mucilage deposition and extrusion in the Arabidopsis seed coat. Plant Cell **13:** 2777–2791.

Pressey, R. (1983). β-Galactosidases in ripening tomatoes. Plant Physiol. **71:** 132–135.

Ridley, B.L., O'Neill, M.A., and Mohnen, D. (2001). Pectins: Structure, biosynthesis, and oligogalacturonide-related signaling. Phytochemistry **57:** 929–967.

Rose, J.K.C., Catalá, C., Gonzalez-Carranza, Z.H., and Roberts, J.A. (2003). Cell wall disassembly. In The Plant Cell Wall, J.K.C. Rose, ed (Boca Raton, FL: CRC Press), pp. 264–324.

Schultz, C., Gilson, P., Oxley, D., Youl, J., and Bacic, A. (1998). GPI-anchors on arabinogalactan-proteins: Implications for signalling in plants. Trends Plant Sci. **3:** 426–431.

Selvendran, R.R., and Ryden, P. (1990). Isolation and analysis of plant cell walls. In Methods in Plant Biochemistry, Vol. 2: Carbohydrates, P.M. Dey and J.B. Harbourne, eds (San Diego, CA: Academic Press), pp. 549–575.

Showalter, A.M. (2001). Arabinogalactan-proteins: structure, expression and function. Cell. Mol. Life Sci. **58:** 1399–1417 (CMLS).

Usadel, B., Kuschinsky, A.M., Rosso, M.G., Eckermann, N., and Pauly, M. (2004). *RHM2* is involved in mucilage pectin synthesis and is required for the development of the seed coat in Arabidopsis. Plant Physiol. **134:** 286–295.

Vincken, J.P., Schols, H.A., Oomen, R.J.F.J., McCann, M.C., Ulvskov, P., Voragen, A.G.J., and Visser, R.G.F. (2003). If Homogalacturonan were a side chain of Rhamnogalacturonan I. Implications for cell wall architecture. Plant Physiol. **132:** 1781–1789.

Western, T.L. (2006). Changing spaces: The *Arabidopsis* mucilage secretory cells as a novel system to dissect cell wall production in differentiating cells. Can. J. Bot. **84:** 622–630.

Western, T.L., Burn, J., Tan, W.L., Skinner, D.J., Martin-McCaffrey, L., Moffatt, B.A., and Haughn, G.W. (2001). Isolation and characterization of mutants defective in seed coat mucilage secretory cell development in Arabidopsis. Plant Physiol. **127:** 998–1011.

Western, T.L., Skinner, D.J., and Haughn, G.W. (2000). Differentiation of mucilage secretory cells of the Arabidopsis seed coat. Plant Physiol. **122:** 345–356.

Western, T.L., Young, D.S., Dean, G.H., Tan, W.L., Samuels, A.L., and Haughn, G.W. (2004). *MUCILAGE-MODIFIED4* encodes a putative pectin biosynthetic enzyme developmentally regulated by *APETALA2*, *TRANSPARENT TESTA GLABRA1*, and *GLABRA2* in the Arabidopsis seed coat. Plant Physiol. **134:** 296–306.

Willats, W.G.T., McCartney, L., and Knox, J.P. (2001a). In-situ analysis of pectic polysaccharides in seed mucilage and at the root surface of *Arabidopsis thaliana.* Planta **213:** 37–44.

Willats, W.G.T., McCartney, L., Mackie, W., and Knox, J.P. (2001b). Pectin: Cell biology and prospects for functional analysis. Plant Mol. Biol. **47:** 9–27.

Windsor, J.B., Symonds, V.V., Mendenhall, J., and Lloyd, A.M. (2000). *Arabidopsis* seed coat development: morphological differentiation of the outer integument. Plant J. **22:** 483–493.

Zheng, H., Kunst, L., Hawes, C., and Moore, I. (2004). A GFP-based assay reveals a role for RHD3 in transport between the endoplasmic reticulum and Golgi apparatus. Plant J. **37:** 398–414.

Zheng, H., Rowland, O., and Kunst, L. (2005). Disruptions of the Arabidopsis enoyl-CoA reductase gene reveal an essential role for very-long-chain fatty acid synthesis in cell expansion during plant morphogenesis. Plant Cell **17:** 1467–1481.